

RESEARCH ARTICLE

A tale of three taxes: photo-gyro-gravitactic bioconvection

C. Rosie Williams* and Martin Alan Bees

School of Mathematics and Statistics, University of Glasgow, Glasgow G12 8QW, UK

*Author for correspondence (chll1@bas.ac.uk)

Accepted 11 February 2011

SUMMARY

The term bioconvection encapsulates the intricate patterns in concentration, due to hydrodynamic instabilities, that may arise in suspensions of non-neutrally buoyant, biased swimming microorganisms. The directional bias may be due to light (phototaxis), gravity (gravitaxis), a combination of viscous and gravitational torques (gyrotaxis) or other taxes. The aim of this study is to quantify experimentally the wavelength of the initial pattern to form from an initially well-mixed suspension of unicellular, swimming green algae as a function of concentration and illumination. As this is the first such study, it is necessary to develop a robust and meticulous methodology to achieve this end. The phototactic, gyrotactic and gravitactic alga *Chlamydomonas augustae* was employed, with various red or white light intensities from above or below, as the three not altogether separable taxes were probed. Whilst bioconvection was found to be unresponsive to changes in red light, intriguing trends were found for pattern wavelength as a function of white light intensity, depending critically on the orientation of the illumination. These trends are explored to help unravel the mechanisms. Furthermore, comparisons are made with theoretical predictions of initial wavelengths from a recent model of photo-gyrotaxis, encouragingly revealing good qualitative agreement.

Key words: bioconvection, swimming, microorganism, phototaxis, gyrotaxis.

INTRODUCTION

The term ‘bioconvection’ was coined by Platt to describe self-sustained pattern formation in shallow suspensions of motile microorganisms that are denser than the fluid in which they swim (Platt, 1961). However, bioconvection is one of the earliest observations of collective behaviours of microorganisms (Wager, 1911). The mechanisms do not necessarily involve communication between the cells. Rather, external influences, such as light and gravity, and self-induced fluid flow bias the cells’ swimming directions. Many microorganism species, such as those belonging to the genus *Chlamydomonas*, are bottom heavy, leading cells to swim upwards on average (gravitaxis); cells tend to accumulate at the upper boundary. If the cells are denser than the surrounding fluid, a horizontal layer with a higher density than the fluid below results. This can lead to Rayleigh–Taylor instabilities, which drive large-scale fluid motion and lead to intricate spatial patterns. Additionally, viscous torques are exerted on each cell by the fluid motion, and the combination of these torques together with those due to gravity is termed gyrotaxis (Kessler, 1984). Gyrotaxis causes cells to swim towards regions of locally downwelling fluid and away from upwelling fluid (Kessler, 1985a; Kessler, 1985b). This is a second mechanism that can lead to instabilities, even in the absence of an upper boundary, as cells swim towards any regions of locally downwelling fluid and their added mass amplifies the downwelling, creating long vertical plumes (Fig. 1A). Both instabilities lead to large-scale pattern formation, and in shallow suspensions, when viewed from above with bright-field illumination, cells form complex patterns with dark regions indicating high cell concentrations (Fig. 1B).

Many genera of microorganisms (e.g. *Chlamydomonas*, *Dunaliella* and *Euglena*) (Nultsch et al., 1971; Foster and Smyth, 1980) also swim towards weak light (positive phototaxis) and away

from strong light (negative phototaxis). This suggests that an optimal, or critical, light intensity exists between these two regimes. Self-shading within a population can occur, where cells closer to the light source absorb and scatter the light; the location of the critical light intensity is determined by the distribution of individuals within the fluid layer. In theory, if the light intensity at an upper source is greater than the critical light intensity, then cells near the source will swim downwards, whereas those further away are shaded by cells above and so swim upwards, resulting in a concentrated, dense sublayer of cells. Only the region below the sublayer is gravitationally unstable. A Rayleigh–Taylor instability caused by the density difference between the cells and the fluid can occur (Vincent and Hill, 1996). Penetrative bioconvection can result, where flows from the unstable region penetrate into the stable region and result in motions that occupy the whole fluid layer, analogous to penetrative thermal convection (Veronis, 1963).

The importance of phototrophic algae for biofuel production should not be overlooked. For economic viability of biofuels from algae, one should look to reduce the energy input into such systems. Photo-gyrotactic behaviour may help to self-concentrate the cells, direct cells away from vertical boundaries (avoiding surface biofouling), provide greater light penetration into deep suspensions, and mix nutrients and promote gas exchange (potentially replacing or enhancing turbulent stirring in algal biofuel systems). The light location might also be adjusted to block bioconvection.

Various models for gravitactic, gyrotactic or phototactic bioconvection have been proposed. Childress and colleagues presented a continuum model for a finite depth suspension of upswimming cells (Childress et al., 1975). The suspension was assumed to be sufficiently dilute so that cell-to-cell interactions could be neglected. Non-Newtonian stresses, such as those associated with swimming strokes, were not considered. The model consisted of

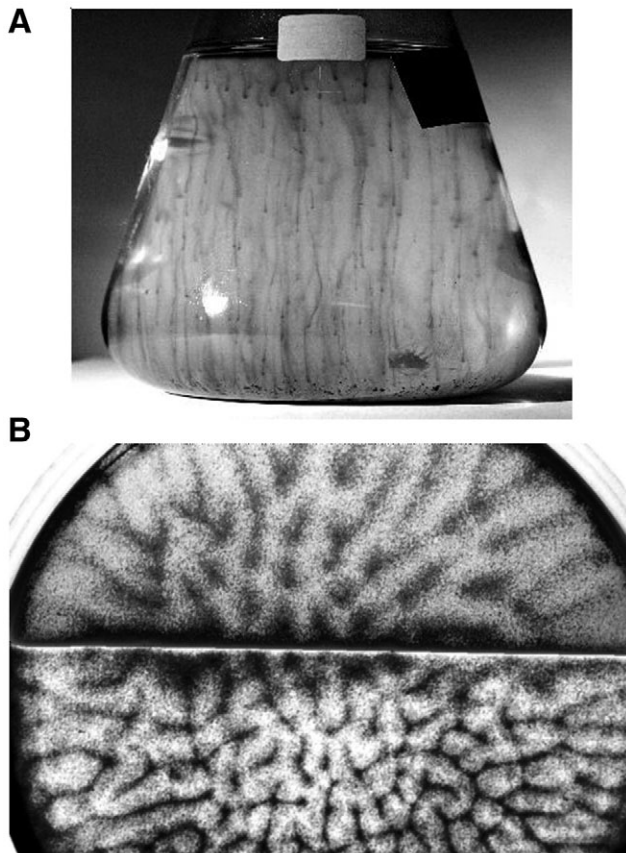


Fig. 1. (A) Gyrotactic plumes in a culture flask. (B) Bioconvection patterns in a Petri dish (depth 0.4 cm; width 5 cm; 10^6 cells cm^{-3}); the illumination is white from below, where the lower half is covered with a red filter (660 nm; contrast enhanced). The two regions display different bioconvection patterns: in the top half, white illumination leads cells to swim upwards, with phototaxis supporting gravitaxis and suppressing gyrotaxis, initiating an overturning instability with broad downwelling structures; in the bottom half, cells do not respond to the red illumination and form finely focused gyrotactic plumes.

the Navier–Stokes equations for the incompressible fluid flow, with an additional term for the negatively buoyant cells, and a cell conservation equation, accounting for advection of the cells by the flow, simple up-swimming and isotropic diffusion. Using linear stability analysis, the dominant initial pattern wavelength was predicted to be limited by the size of the container (zero critical wavenumber). However, the discovery of gyrotaxis demonstrated the incompleteness of this description and injected new energy into theoretical investigations, with subsequent models explicitly including gyrotaxis (with gravitaxis implicit). The first models calculated cell swimming direction deterministically and used constant isotropic diffusion (Hill et al., 1989). Later, a refined continuum model was developed (Pedley and Kessler, 1990), with a stochastic gyrotactic description from which the flow-dependent mean cell swimming direction and diffusion tensor could be derived. This model was analysed for a layer of finite depth (Bees and Hill, 1998); finite initial pattern wavelengths were predicted for sufficient gyrotaxis. In the first model of phototactic-only cells (Vincent and Hill, 1996), cells simply swam upwards or downwards depending on the local light intensity (see Ghorai and Hill, 2005). Finally, three models have been constructed that include phototaxis, gravitaxis

and gyrotaxis in a continuum description of bioconvection (Williams and Bees, 2011) [in the spirit of Pedley and Kessler (Pedley and Kessler, 1990)]. These represent the first rational models of photo-gyrotaxis and mark a substantial development in the theory of bioconvection under illumination.

There has not been a substantial amount of quantitative experimental work to accompany the theoretical developments; early studies and observations were qualitative in nature (Wager, 1911; Kessler, 1984; Kessler, 1985b; Kessler, 1986). More recently, controlled experiments quantified the initial and final wavelengths of patterns as a function of cell concentration and depth in a shallow suspension of *Chlamydomonas augustae* (Bees and Hill, 1997) (no phototaxis, as cells are effectively in the dark). The initial wavelengths could be compared with model predictions (Bees and Hill, 1998). Finally, Cziráok and colleagues investigated bioconvection in suspensions of aerotactic bacteria (Cziráok et al., 2000). Combined phototaxis and gravitaxis has been probed in tracking experiments (Kessler et al., 1992) with either weak or strong horizontal irradiance, with the conclusion that ‘any complete discussion of phototaxis in a microorganism that is also gravitactic must take both responses into account’.

The aim of this investigation was to analyse experimentally the effects of light intensity and concentration on the initial wavelength of the bioconvection pattern in a repeatable and precise manner. This is the very first quantitative study on the effect of light on bioconvection patterns. The initial instability that forms before any higher-order, non-linear effects occur is of particular interest as this can be compared directly with theoretical predictions (Williams and Bees, 2011) on photo-gyrotactic bioconvection. The methodology has been developed from the literature (Bees and Hill, 1998; Cziráok et al., 2000), with some key modifications and extensions. In particular, a novel, automated method of mixing was designed in an attempt to decrease the effects of variable mixing that occur between experiments. Furthermore, this is the first study of its kind to systematically repeat experimental runs, using the same cells, in order to provide a solid statistical basis for the results and mechanistic descriptions. Additionally, each experiment was repeated using different cells to assess whether the trend was repeatable. Fourier analysis was used to extract the dominant initial pattern wavelength as a function of concentration and light intensity, with red and white illumination from above and below. This study concludes with a thorough discussion of the mechanisms responsible for the trends that are observed, and a comparison with theoretical predictions, where, encouragingly, good agreement is found.

MATERIALS AND METHODS

Culture, depth and concentration

The experiments were performed with the motile green alga *Chlamydomonas augustae* Skuja 1943, strain CCAP 11/51B (formerly listed as *C. nivalis* Wille), suspended in Bold’s basal medium (BBM). Cultures were stored in 500 ml conical flasks, sealed with cotton wool and covered in tin foil to avoid contamination. Illumination was from above using bright white fluorescent strip lights (16 h:8 h light:dark cycle; intensity of 1900 lx just above the cultures). Cultures were sub-cultured every 4 weeks and used in experiments after 2–4 weeks. The cells can be concentrated by placing sterile absorbent cotton wool in the neck of the flask; cells swim upwards through the cotton wool and accumulate at the top in the dark. After 2 days, a pipette was used to extract a known volume of concentrated culture, which was placed in a Petri dish (diameter 5.2 cm). To avoid adhesion to the Petri dish, new dishes were washed with distilled water and then culture,

followed by concentrated suspension, and left for 24 h. The depth in the centre of the dish was measured using a microscope focus, calibrated with glass slides measured with a micrometer. Concentration was measured using the mean of five colorimeter measurements (WPA CO7500 colorimeter, Cambridge, UK, 590 nm; BBM reference; calibrated *via* a haemocytometer, using Beer's law to find a linear relationship between absorbance and concentration; non-linearity for high concentrations was avoided by dilution).

Mixing and lighting

For quantitative studies of bioconvection patterns, a uniform distribution of cells is required in the Petri dish at the start of the experiment, to standardize initial conditions. In previous studies, cultures were mixed by hand (Czirók et al., 2000), which allowed patterns to vary between experiments [fig. 8 in Bees and Hill (Bees and Hill, 1997)] due to the inherent ability of the cells to self-concentrate in a range of flows. Here, an automated mixing method was designed and implemented to standardize mixing to an acceptable degree between experimental runs. A vortex mixer (Jencons PLS VX100, West Sussex, UK) was used with a flat head attachment to support the culture in the Petri dish positioned on a light box (for light from below) or on a counterbalanced board (for light from above) on top of the mixer. The vortex mixer was set to a slow 200 r.p.m., creating a swirling, sloshing motion in the culture that appeared to mix the suspension. Mixing was deemed acceptable if the pattern appeared to form uniformly, appeared after the effects of mixing had subsided and did not obviously follow streamlines. Investigation showed that an initial thorough mixing followed by a rest period and then a further brief mixing satisfied these requirements. The mixing motion varied a little with the position of the illumination. Parameters for each experiment are summarized in Table 1, where consecutive pairs of mixing and waiting times (m_i, t_i) are indicated.

Lighting consisted of either a red or cold white uniform diffuse LED array [Advanced Illumination, Rochester, VT, USA; no significant heating; for spectra, see Williams (Williams, 2009)]. All other lights were extinguished. The PC-controlled illumination intensity was stated in lx on the surface of the light box, calibrated with a light meter. For light from below, the culture dish was fixed within a large Petri dish on the light box, for stability, with a lid to reduce contamination and limit evaporation. This in turn was attached to the vortex mixer, with a tripod-mounted camera overhead. For illumination from above, a board was employed with a Petri-dish-sized hole at one end; the culture dish was inserted in the hole with the light strapped to the top, the board was attached to the mixer and counterbalanced, and the inverted camera was placed below.

Table 1. Summary of the experimental mixing protocol

Experiment	Light type	Light orientation	(m_i, t_i) pairs (s)
RA	Red	Above	(4, 10), (2, 10)
CA	White	Above	(5, 2), (3, 4), (2, 10)*
CB	White	Below	(2, 10), (1, 12)
LA(1,2,3)	White	Above	(5, 2), (3, 4), (2, 12)
LB(1,2,3)	White	Below	(3, 10), (1, 12)

A, illumination from above; B, illumination from below; C, concentration experiment; L, white light intensity experiment; R, red light.
(m_i, t_i), sequence of pairs of mixing and waiting times: either (m_1, t_1), (m_2, t_2) or (m_1, t_1), (m_2, t_2), (m_3, t_3) in cases where more mixing was required. The asterisk indicates that the final waiting time was flexible, to avoid missing initial pattern formation.

Varying concentration in the suspension

Depth and illumination were kept constant for experiments that involved varying concentration. Eight experimental runs were performed with the maximum concentration, C_{\max} . A controlled dilution was obtained by replacing 2 ml of culture in the Petri dish with 2 ml of BBM (equilibrated temperature), without repositioning the culture. The culture was thoroughly mixed and left on the light box to re-adjust for 10 min before performing another eight experimental runs. This procedure was repeated, with 2 ml replaced each time, until pattern formation was significantly attenuated; typically, five dilutions were required.

Image capture and analysis

For each experimental run (mixing plus image capture), 30 images were captured (Camtek low-light-sensitive BW CCD, Bagshot, Surrey, UK) at intervals of 2 s. For each set of parameter values, N represents the number of experiments (separated by 30 s) performed with the same cells. Light intensity, I , was initially set at 645 lx (10% of maximum) and was increased in increments of 15% of the maximum.

Fourier analysis was employed to extract the dominant wavelength in each of the recorded images [for details and references see Bees and Hill (Bees and Hill, 1997) and Czirók et al. (Czirók et al., 2000)]. In brief, using software written in the graphics package IDL (RSI, Berkshire, UK), the first image was subtracted from the stack of images to extract unwanted information (the walls of the dish, imperfections and uneven lighting); a Hahn windowing function was used to eliminate the effects of the sharp edges of the image before fast Fourier transformation (FFT). The FFT takes a real, two-dimensional image array and returns a complex array of the same size containing amplitude and phase information, from which a discrete Fourier spectrum, $G(k)$, for wavenumber k can be computed, yielding the dominant wavenumber, k_d (the peak of the fit). Two functions have been proposed to fit the spectrum (using least-squares), an unnormalized double Gaussian distribution (Bees and Hill, 1997) and a function with power-law decay for both small and large wavenumbers (Czirók et al., 2000) of the form:

$$\ln[G(k)] = \alpha \ln(k) - \ln(k_d) - \beta \ln(k) + c, \quad (1)$$

where α , β and c are fitting parameters (α and β are exponents for small and large wavenumbers). This is equivalent to separating logarithms and writing $G(k) \sim k^{-\alpha-\beta}$ when $k < k_d$, and $G(k) \sim k^{\alpha-\beta}$ when $k > k_d$.

For the images herein, the double logarithmic function better fitted the data than the double Gaussian and thus was used throughout (sum modulus and Kolmogorov–Smirnov statistics were smaller) (Williams, 2009). An example of the fitting is shown in Fig. 5. Very occasionally, when poor-fitting statistics were obtained, the first most unstable wavenumber was estimated directly from the spectrum (very few cases). Wavenumber can be converted to wavelength as follows: $\lambda = W_1/k_d$, where W_1 is the image width (cm). The initial dominant wavenumber and wavelength are denoted k_0 and λ_0 , respectively, and were identified as such if the associated Fourier spectrum density was sufficiently greater than the noise and grew with time. Finally, the data easily satisfy the Nyquist criterion of at least two pixels per oscillation.

Statistical analysis

Linear regression analyses were performed (Sigma Plot 8.0, Systat Software, London, UK) on all data points from each experimental run (not just the mean wavelength). Correlation coefficients were found and t -tests were performed to analyse the probability of

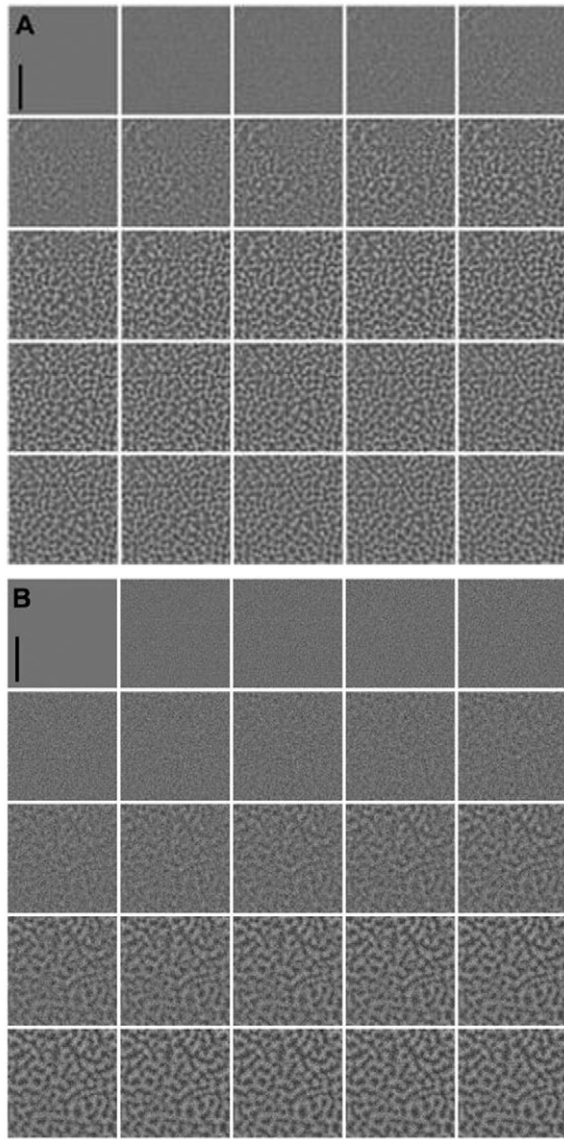


Fig. 2. Sample images from experiment CA (white light illumination from above, $I=645$ lx; $H=0.306$ cm; $W=2.47$ cm). (A) $C=8.11 \times 10^6$ cells cm^{-3} ; (B) $C=3.33 \times 10^6$ cells cm^{-3} . Images were captured every 2 s, starting 10 s after mixing. Scale bars, 1 cm.

incorrectly concluding the existence of an association between the dependent and independent variables. Unpaired t -tests were also used to establish whether differences in mean wavelength for different parameters were significant.

RESULTS

To facilitate easy discussion of the experimental results in the next section, we shall employ the experimental naming convention used in Table 1.

Exploring the effects of concentration on initial pattern wavelength

Fig. 2 shows two examples of the evolution of bioconvection patterns with illumination from above at 645 lx, for different concentrations. There is a clear difference in the patterns formed: for the higher concentration, the pattern has an earlier onset and a smaller wavelength compared with the lower concentration.

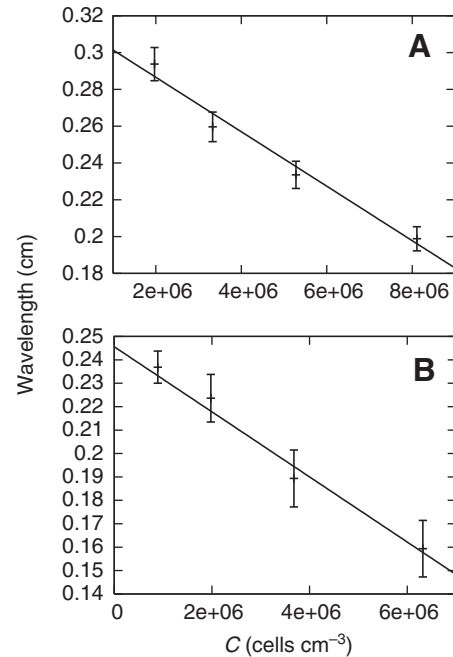


Fig. 3. The effects of concentration on dominant initial pattern wavelength. (A) Experiment CA, culture illuminated from above with a white light ($I=645$ lx; $H=0.306$ cm). (B) Experiment CB, culture illuminated from below with a white light ($I=645$ lx; $H=0.345$ cm).

Results for the effect of concentration on initial pattern wavelength are shown in Fig. 3, where the data points are the mean of eight separate measurements of the same cells and the error bars indicate the standard error of the means. For light from above and below, results show that increasing concentration decreases the initial wavelength of the instability. In the absence of any other obvious trend, a linear regression analysis is used to fit a straight line to the data (Table 2).

The correlation coefficients are both <-0.7 . The low P -values are highly significant and indicate that it is very unlikely that there is not a correlation between the concentration and initial wavelength. Results from unpaired t -tests between consecutive concentrations for light from above indicate that the change in pattern wavelength with increasing concentration is significant ($P<0.05$). For light from below, consecutive concentrations give slightly insignificant P -values, but non-consecutive concentrations give highly significant values (for example, testing the first and the third concentration data points). Thus, together with the linear regression analysis, we conclude that there is negative correlation between concentration and initial pattern wavelength.

Does red light illumination affect the initial pattern wavelength?

There is a considerably reduced response to light wavelengths greater than 550 nm in the action spectra for the photo response of *Chlamydomonas* [*C. reinhardtii* (Nultsch et al., 1971)]; the photoresponse to red light is small. By illuminating a culture from below using red light of wavelength 660 nm, we investigated whether the initial pattern wavelength varies with light intensity. An example of the resulting patterns formed with $I=101$ lx and a contour plot of the Fourier spectra with time are shown in Fig. 4, and graphs of Fourier density are plotted in Fig. 5. In this particular example, we note that the pattern does not appear everywhere in

Table 2. Summary of linear regression statistics for concentration experiments

Experiment	Linear fit	r	r^2	P (constant)	P (gradient)
CA	$0.316-1.48 \times 10^{-8}C$	-0.849	0.721	<0.0001	<0.0001
CB	$0.246-1.39 \times 10^{-8}C$	-0.704	0.496	<0.0001	<0.0001

C , concentration; r , correlation coefficient; r^2 , coefficient of determination; P (constant), P -value associated with the constant in the linear fit; P (gradient), P -value associated with the gradient coefficient in the linear fit (calculated with ANOVA).

the dish at the same time, possibly due to a remnant of mixing driven swirling. The dominant wavenumber can still be extracted, and the double log fit is accurate.

There is no apparent trend in the wavelengths as the red light intensity is varied (Fig. 6). The correlation coefficient for linear regression, $r=-0.0957$ ($r^2=0.009162$), is very small and implies that there is no significant correlation between the variables, and the corresponding P -values support this. In addition, no significance was found comparing the mean wavelength for different light intensities using sets of unpaired t -tests. This lack of response implies that illumination by red light is practically equivalent to no illumination, i.e. $I=0$ lx.

White light illumination from below

A significant phototactic response is elicited in *C. reinhardtii* for wavelengths between 370 and 550 nm (Nultsch et al., 1971), with a maximum at 503 nm and shoulder at 443 nm. Covering this range with the white LED array, results for the initial pattern wavelength as a function of illumination from below are shown for three independent experiments, with different cultures, in Fig. 7, with concentrations of 5.35×10^6 , 5.18×10^6 and 9.46×10^6 cells cm^{-3} ($N=6$, 8 and 8, respectively). We denote these experiments LB1, LB2 and LB3, respectively.

Results in Fig. 7 show the same trends: a decrease in initial wavelength as light intensity is increased to 2020 lx followed by an increase as intensity is increased to 2710 lx, and then what appears to be a stabilization of wavelengths as light is increased further, with wavelengths approximately constant beyond 2710 lx. If the data for red light for a similar concentration were included as $I=0$, it would also fit with the trend of decreasing wavelength as I is increased to 2020 lx. As expected, there is some variability in the quantitative values of the mean wavelengths for different graphs, which may be due to the fact that slightly different concentrations are used, and cell behaviour may vary (i.e. variations in life or daily cycles). The trends found in these experiments are non-linear overall but appear to have quasi-linear regions. Thus we performed a linear regression separately on the first three points (for light intensities $I=645$, 1330 and 2020 lx) and then on the following four points ($I=2710$, 3390, 4080 and 4770 lx), denoting the first three data points LB1a, LB2a and LB3a and the latter four points LB1b, LB2b and LB3b, for the three experiments, respectively. The linear fits and corresponding statistics are presented in Table 3.

For the first linear fit, experiment LB1a shows the strongest negative correlation, whereas LB2a and LB3a show weaker correlations. The corresponding ANOVA gave a significance level of $P<0.002$ for the probability of being wrong in concluding that

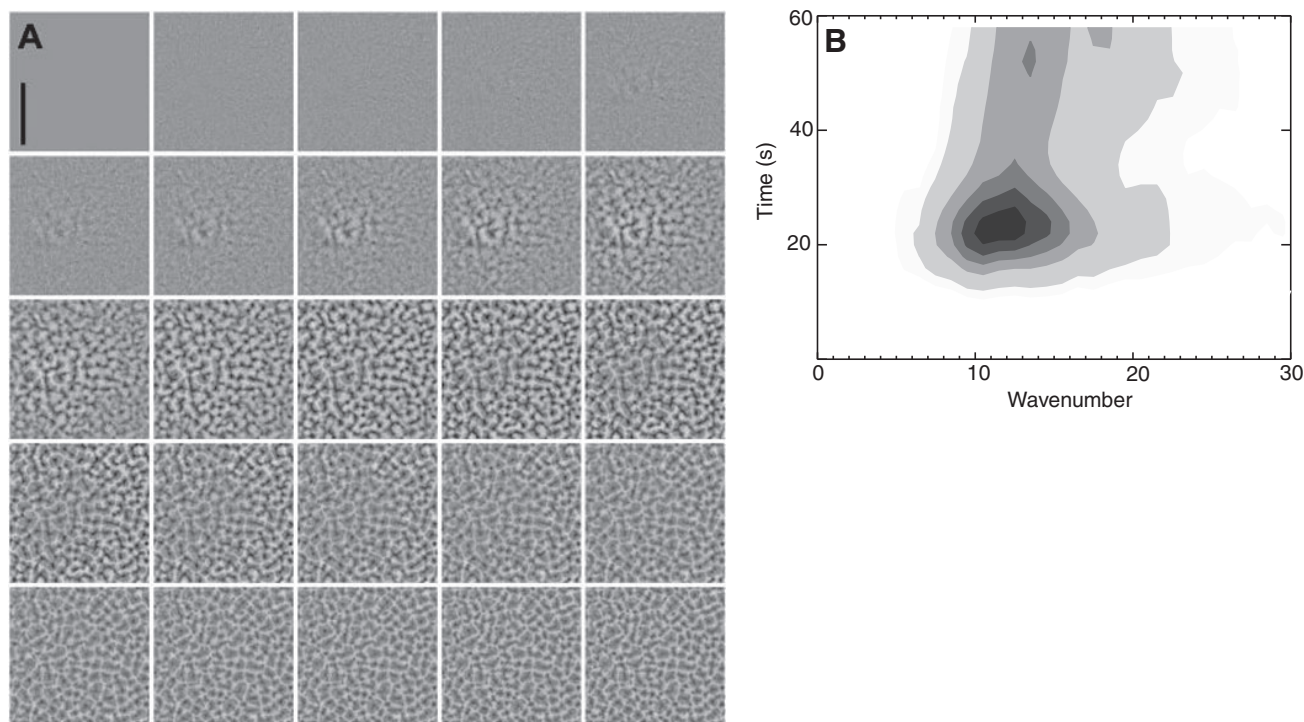


Fig. 4. Sample results from experiment RA, with red light illumination from above ($I=101$ lx; $C=5.05 \times 10^6$ cells cm^{-3} ; $H=0.306$ cm; $W=2.33$ cm). (A) Images were captured every 2 s, starting 10 s after mixing. Scale bar, 1 cm. (B) Contour plot of the Fourier spectrum, where time is measured from the start of image recording (not the time since mixing).

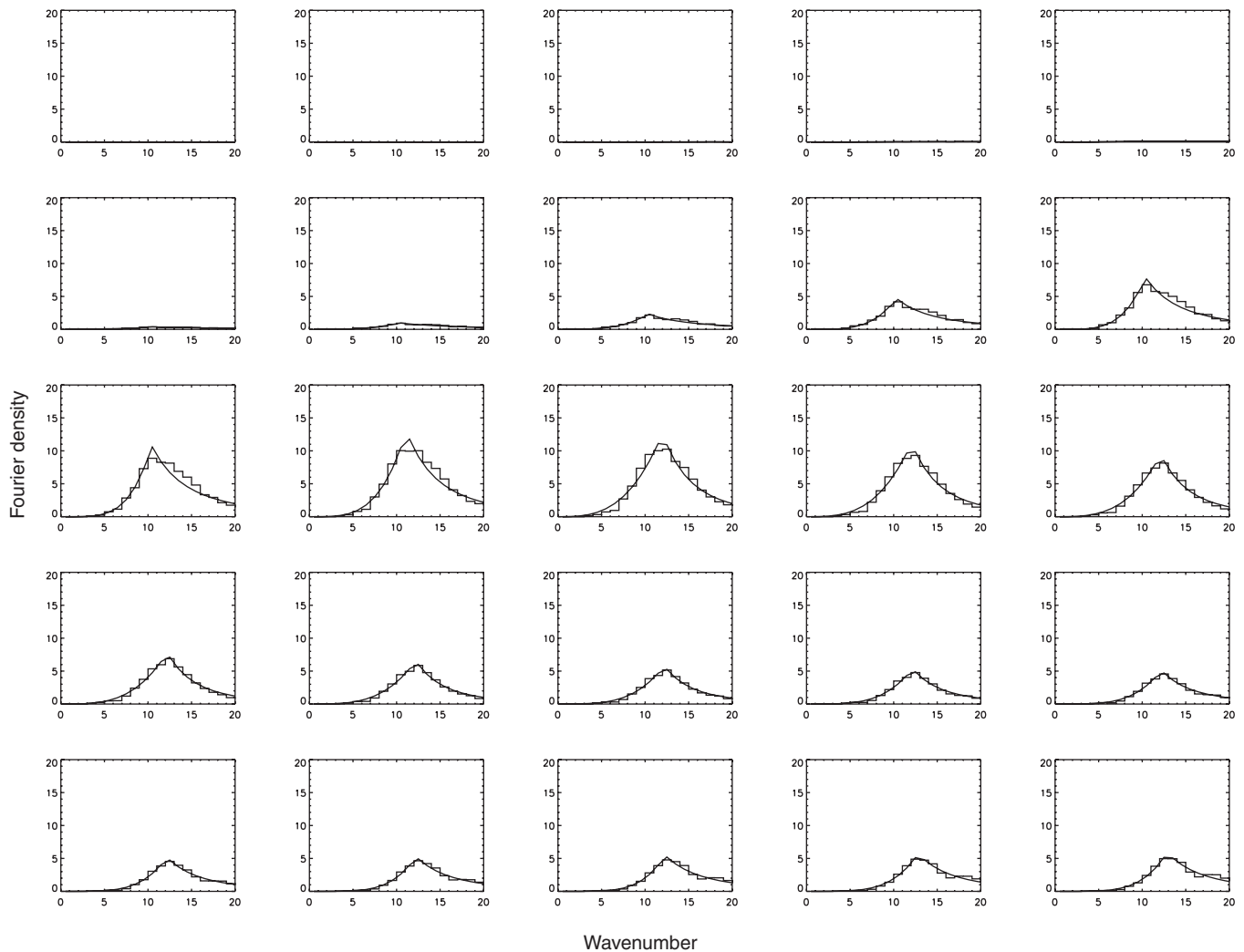


Fig. 5. Fourier spectra from experiment RA, with red light illumination from above ($I=101$ lx; $C=5.05 \times 10^6$ cells cm^{-3} ; $H=0.306$ cm). Spectra were computed every 2 s, starting 10 s after mixing ended. The horizontal axis is wavenumber and the vertical axis is Fourier density. Histograms represent binned data of the FFT spectrum of each processed pattern image, whereas the curves are produced from fitting Eqn 1.

there is an association between light intensity and initial wavelength. Furthermore, unpaired t -tests on the first and the last data points in LB1a, LB2a and LB3a were highly significant in every case ($P < 0.05$). Thus we conclude that there is evidence of a significant negative linear relationship between light and wavelength for $I \leq 2020$ lx.

For the second linear fit, the correlation coefficients are very low, especially for the more concentrated cells in LB3b and, hence, there is no evidence of a correlation between light intensity and wavelength for $I > 2710$ lx. In all cases, the probability in being wrong in concluding that there is a relationship between the two variables is very high. Such statistics imply that these data sets are uncorrelated and that there is not sufficient evidence to conclude that light intensity and initial wavelength vary together in an associated way. Thus, averaging all data points for $I \geq 2710$ lx in LB1b, LB2b and LB3b gives $\lambda_{\text{WB1}} = \lambda_{\text{WB2}} = 0.1600$ (s.d. = 0.0115 and 0.0184, respectively) and $\lambda_{\text{WB3}} = 0.1582$ (s.d. = 0.0147).

The rise in λ_0 between $I = 2020$ lx and $I = 2710$ lx was examined using t -tests and found to be statistically significant in experiments LB1 and LB3 ($P < 0.05$), but not significant in LB2. From this, together with the aforementioned statistical analysis, we conclude

that with increasing light intensity the initial wavelength decreases in a linear fashion, increases and stays at approximately the same level thereon in two cases, and in the third case, decreases, stops decreasing and stays at approximately the same level. We shall interpret these results mechanistically in the Discussion.

White light illumination from above

The initial pattern wavelength for cultures illuminated from above were explored in three experiments (using different cells), LA1, LA2 and LA3, with depth $H = 0.306$ cm and concentrations of 5.05×10^6 , 4.86×10^6 and 5.69×10^6 cells cm^{-3} , respectively. Eight experimental runs ($N = 8$) were conducted for each light intensity to establish the mean wavelength λ_0 .

Results in Fig. 8, for initial wavelength *versus* light intensity, show the same trend: as light increases from 645 to 1330 lx, the initial wavelength increases; beyond $I = 2020$ lx, λ_0 decreases. If the data for illumination with red light for a similar concentration were included ($I = 0$ lx, $\lambda_0 = 0.19$ cm), it would be consistent with the trend of increasing λ_0 for small I . As for illumination from below, the curves are qualitatively similar, but there are quantitative differences between the data sets due to the distinct cell populations.

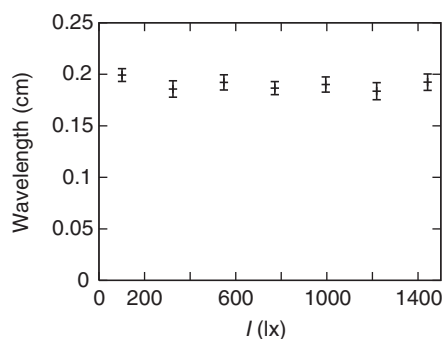


Fig. 6. The effect of red light from above on dominant initial pattern wavelength ($H=0.306$ cm; $C=5.05 \times 10^6$ cells cm^{-3}). Each point represents the mean of eight runs of experiment RA; error bars are \pm s.e.m.

Comparing the mean wavelengths for $I=675$ and 1330 lx using an unpaired t -test, it was found that the increase in wavelength was significant in every experimental case ($P < 0.05$). Furthermore, a linear regression analysis was performed excluding the first data point, $I=645$ lx. The linear regression statistics are shown in Table 4. The negative correlation was strongest in LA1, and not as pronounced in LA2 and LA3. Using an unpaired t -test, the difference in λ_0 for $I=1330$ and 4770 lx was found to be significant in all three experiments ($0.0001 < P < 0.0013$). This, together with the small P -values found for all data sets (using ANOVA) for the probability of being wrong in concluding an association between the variables, indicates that the decrease in initial wavelength as I increases from 1330 to 4770 lx is a significant trend that is approximately linear.

Exploring the time to pattern formation

The time from mixing to pattern onset, t_0 , as a function of light intensity was investigated. For red light, eight runs from experiment RA, where $I=325$ lx, provided the mean t_0 . For white light from above and below, two sample experiments, LA1 and LB1, were chosen and the mean t_0 was calculated over eight runs for each light intensity (Fig. 9).

For experiment LB1, the time to pattern formation increased from $t_0=28$ s at $I=645$ lx to a maximum of $t_0=36$ s at $I=2710$ lx. As I increased above 2710 lx, the time to pattern formation then dipped a little to 34 s. For experiment LA1, we see a similar pattern of behaviour except that the maximum occurs at 3390 lx with $t_0=41$ s. With red light, pattern formation occurred after 21 s, earlier than for any white light. If red light is treated as $I=0$, then this data point supports the above trends (Fig. 9).

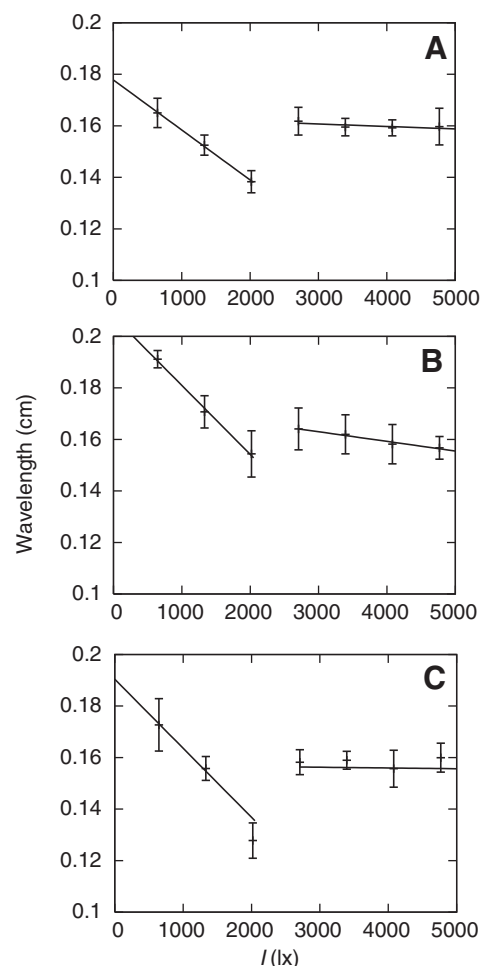


Fig. 7. The effect of white light illumination from below on dominant initial pattern wavelength ($H=0.306$ cm). (A) $C=5.35 \times 10^6$ cells cm^{-3} ; (B) $C=5.18 \times 10^6$ cells cm^{-3} ; (C) $C=9.46 \times 10^6$ cells cm^{-3} . Each point represents the mean of six runs of experiment LB1 and eight runs of experiments LB2 and LB3; error bars are \pm s.e.m. Linear regression fits have been plotted for all experiments, separately for the first three or last four points in each data set.

DISCUSSION

For a given light intensity, when the culture was illuminated from above or below, the initial wavelength of the most dominant mode, λ_0 , decreased as concentration increased. This is consistent with the results of Bees and Hill (Bees and Hill, 1997), who measured wavelengths of a similar order, supporting the hypothesis that

Table 3. Summary of linear regression statistics for experiments with illumination from below

Experiment	Linear fit	r	r^2	P (constant)	P (gradient)
LB1a	$0.178-1.94 \times 10^{-5}I$	-0.720	0.518	<0.002	<0.002
LB2a	$0.208-2.68 \times 10^{-5}I$	-0.650	0.422	<0.002	<0.002
LB3a	$0.190-2.68 \times 10^{-5}I$	-0.613	0.376	<0.002	<0.002
LB1b	$0.164-9.62 \times 10^{-7}I$	-0.066	0.0043	<0.0001	0.760
LB2b	$0.174-3.74 \times 10^{-6}I$	-0.166	0.0274	<0.0001	0.391
LB3b	$0.157-2.87 \times 10^{-7}I$	-0.015	0.0002	<0.0001	0.934
CB	$0.246-1.39 \times 10^{-8}C$	-0.704	0.496	<0.0001	<0.0001

C , concentration; I , light intensity; r , correlation coefficient; r^2 , coefficient of determination; P (constant), P -value associated with the constant in the linear fit; P (gradient), P -value associated with the gradient coefficient in the linear fit (calculated with ANOVA).

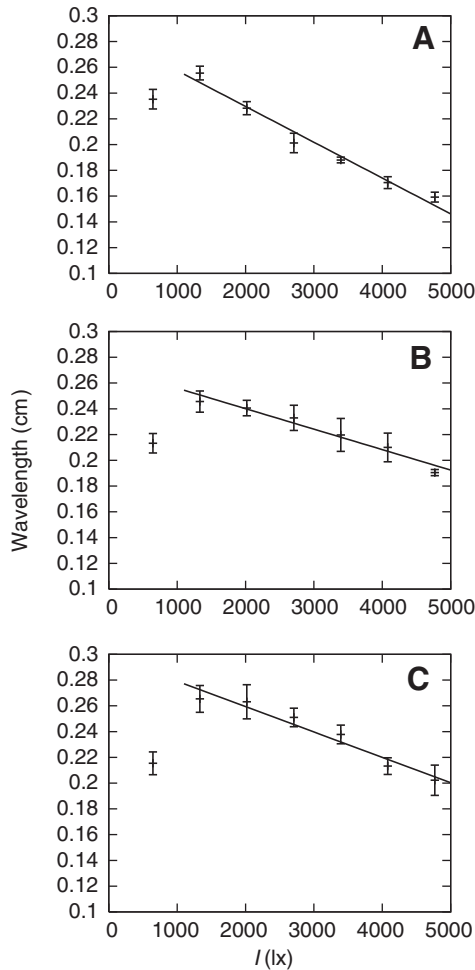


Fig. 8. The effect of white light illumination from above on dominant initial pattern wavelength ($H=0.306$ cm). (A) $C=5.05 \times 10^6$ cells cm^{-3} ; (B) $C=4.86 \times 10^6$ cells cm^{-3} ; (C) $C=5.69 \times 10^6$ cells cm^{-3} . Each point represents the mean of eight runs of experiment LA; error bars are \pm s.e.m. Linear regression fits have been plotted for all experiments (excluding the first data point at $I=645$ lx in each).

increased gyrotaxis for higher cell concentrations encourages more focused and closely packed plumes.

The insensitivity of initial wavelengths to the red light illumination shows that, at least in terms of pattern formation, the cells do not exhibit a photo-response to light of wavelength 660 nm. This observation is consistent with data on individuals (Nultsch et al., 1971). Hence, red light is practically equivalent to no illumination. The mean wavelength over all intensities for red light is $\lambda_0=0.19$ cm, which is of the same magnitude as similar experiments, although a little smaller [57.4% of the reported value

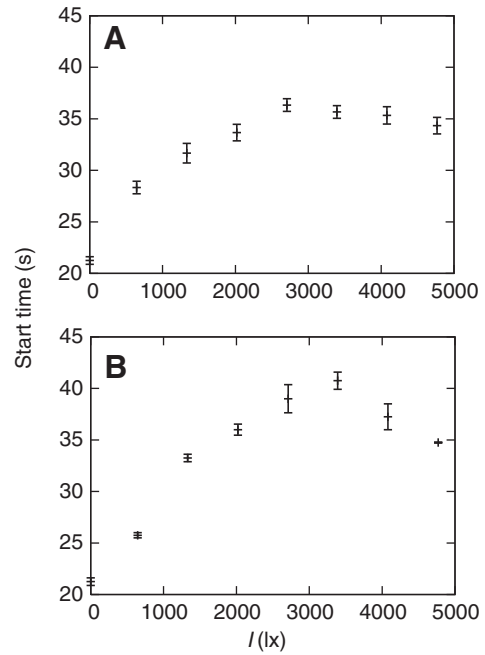


Fig. 9. Mean initial start time, t_0 , plotted against light intensity for experiments (A) LB1 and (B) LA1. The mean start time for $I=325$ lx for the red light experiment RA is included as $I=0$ lx: red light has negligible effect on photo-motility. $H=0.306$ cm; images were captured every 2 s, starting 12 s after mixing.

for concentration $C=3.6 \times 10^6$ cells cm^{-3} and depth $H=0.324$ cm in Bees and Hill (Bees and Hill, 1997)].

We have reported the first statistically significant trends for initial pattern wavelength as a function of white light intensity for cultures illuminated either from above or below. The results for both light orientations were found to be repeatable. Distinct transitions were observed as the light intensity was increased. To explain these results, we recall that there is a competition between bottom-heavy induced upswimming (gravitaxis), gyrotaxis due to viscous and gravitational torques, and phototaxis towards/away from weak/bright light, distinguished by the critical light intensity, I_c .

For the case of illumination from below (Fig. 7), the initial wavelength decreased linearly as light intensity was increased from $I=645$ to 2020 lx, then increased as intensity increased from 2020 to 2710 lx, and remained constant for $I \geq 2710$ lx. From these results, it would appear that $2020 \leq I_c \leq 2710$. For very weak illumination, cells generally swim upwards, but the probability density function (pdf) for the orientation of cells will be less biased upwards as I increases, and cells will be more responsive to viscous torques, leading to stronger gyrotaxis (swimming towards regions of downwelling fluid), more focused plumes and thus smaller wavelength instabilities. (Note that gyrotaxis can induce linear

Table 4. Summary of linear regression statistics for experiments with illumination from above

Experiment	Linear fit	r	r^2	P (constant)	P (gradient)
LA1	$0.285-2.78 \times 10^{-5}I$	-0.915	0.837	<0.0001	<0.0001
LA2	$0.272-1.59 \times 10^{-5}I$	-0.604	0.351	<0.0001	<0.0001
LA3	$0.299-1.97 \times 10^{-5}I$	-0.688	0.474	<0.0001	<0.0001

I , light intensity; r , correlation coefficient; r^2 , coefficient of determination; P (constant), P -value associated with the constant in the linear fit; P (gradient), P -value associated with the gradient coefficient in the linear fit (calculated with ANOVA).

instabilities of small wavelength even in suspensions of uniform concentration.) With illumination from below for $I < I_c$, shading does not permit a steady state with a maximum within the suspension. For I just below I_c , photo-gyrotaxis plays a critical role as short wavelength instabilities develop before gravitationally stable steady states are attained (cells concentrated at the bottom). For $I > I_c$, cells typically swim upwards, leading to accumulations at the upper surface and overturning instabilities with circulation associated with the whole fluid layer (λ_0 does not change significantly with I). It is the switch from a photo-gyrotactic instability from an evolving basic state to an overturning instability from photo-gravitaxis that provides the rapid change in wavelengths in Fig. 7.

With light from above (Fig. 8), the initial wavelength increased a little with light intensity between 645 and 1330 lx, and decreased between 1330 and 4700 lx. To explain the former, for weak illumination the cells swim towards the light on average and, hence, gravitaxis is supported by phototaxis. Greater illumination leads photo-gravitaxis, with large wavelength instabilities, to dominate over more focused, gyrotactic instabilities. When I is increased above I_c , negative phototaxis is sufficient to overcome negative gravitaxis (Häder, 1987), and the cells near the top of a uniform suspension swim downwards, whereas those lower down swim upwards because of shading, in theory creating a concentrated sublayer somewhere within the full layer. Because the sublayer is denser than the suspension above and below, a stable region overlies an unstable region. We propose a dual explanation for the decrease in pattern wavelength as white light intensity increases further. Firstly, the disposition of cells near the light source to swim downwards as the intensity increases broadens the orientation pdf, thus increasing gyrotactic focusing, which decreases λ_0 . Secondly, as light intensity increases, the unstable region below the sublayer decreases in size, stabilizing large wavelength instabilities more than small. To determine the I_c from above, note that zero phototaxis typically occurs at two points: $I=0$ and I_c . Therefore, one might expect λ_0 to be the same at both. Of course, self-shading within the suspension, particularly at the top, complicates the argument and limits the accuracy of this prediction, although the results are consistent with illumination from below, yielding a value of $I_c \approx 3000$ lx (Fig. 8).

The start time of pattern formation, t_0 , was computed as a function of illumination from above or below. For red light, instabilities typically are seeded by unstable cell concentration profiles and gyrotaxis supports the process. For low light intensities with light from below, cells swim downwards as light intensity increases, delaying the time to form an unstable density gradient and thus initiate instability, despite the amplified gyrotaxis. For $I > 2710$ lx, overturning instabilities near the upper boundary are the dominant mechanisms, taking a while to form as they will not be supported by gyrotaxis. Similarly, illumination from above presents an analogous competition of taxes.

Comparison with theoretical predictions of photo-gyrotactic bioconvection

An aim of this study is to present results that can be compared with current and future theoretical predictions. In theory, initial wavelength predictions can be compared. However, such a comparison is rarely straightforward (see below) and there are some key issues that need to be addressed: have the effects of mixing sufficiently diminished before pattern formation begins; and has the cell distribution approached the theoretical steady state before pattern onset? To answer the first question, we assume that the Petri dish is in solid body rotation with angular velocity $|\Omega|$ until the mixing stops and the container instantaneously comes to rest (Hill et al.,

1989; Bees and Hill, 1997). The time for spin down and decay of fluid motion is $O(E^{-1/2}|\Omega|^{-1})$, where $E = \nu(\rho/H^2)^{-1}$ is the Ekman number, ν is the viscosity and H is the layer depth (Acheson, 1990). In our case, $|\Omega| = 21 \text{ s}^{-1}$ (using the speed of the vortex mixer), and we calculate $E = 5.3 \times 10^{-3}$, thus $O(E^{-1/2}|\Omega|^{-1}) = 0.65 \text{ s}$. Because pattern formation starts after tens of seconds, we conclude that the flow is likely to have diminished sufficiently. For a mean cell swimming speed of $63 \mu\text{m s}^{-1}$ (Hill and Häder, 1997) with an upward bias of 56% (Bees et al., 1998) and a layer depth of 0.3 cm, a cell takes 43 s to swim half the depth. This implies that not all the cells will have had sufficient time to form the steady states used in the models. However, some qualitative comparisons can still be drawn.

Recent theory employs linear stability analyses to assess the initial pattern wavelengths of instabilities in both gyrotactic-only (Pedley and Kessler, 1990; Bees and Hill, 1998) and phototactic-only cells (Vincent and Hill, 1996). Results for red light can be compared with gyrotaxis-only models, and trends for the effects of white light on initial bioconvection wavelengths can be compared with predictions from photo-gyrotactic models (Williams and Bees, 2011). Three models for photo-gyrotaxis have recently been presented and explored in detail (Williams and Bees, 2011). In Model A, the mean cell swimming speed decreases linearly with $|I - I_c|$, with zero mean swimming speed at the critical light intensity, I_c . The mean cell swimming direction is determined separately by balancing gravitational and viscous torques in a stochastic formulation. In Model B, each cell's deterministic-stochastic ratio varies linearly with I , effectively *via* its centre-of-mass offset: at $I = I_c$, the gravitational torque is zero and in the absence of viscous torques the cell is equally likely to swim in all directions; for $I < I_c$, the cell swims upwards on average, obtaining the measured value for $I = 0$. In Model C, an effective phototactic torque (e.g. due to an active asymmetric adjustment of the flagellar beat) complements the existing gravitational and viscous torques; the model displays evidence of novel non-hydrodynamic modes. Because fluid flow was integral to the results obtained experimentally, only comparisons with Models A and B are made here: a layer of finite depth illuminated from above is studied, where key parameters are the scaled layer depth (d), the ratio of the light intensity at the source (I_s) to the critical light intensity, $\chi = I_s/I_c$, and the Rayleigh number $Ra = \nu g \Delta \rho H^3 d N / (\nu \rho V_n^2 \tau)$, which is a ratio of the destabilising to stabilising forces (see Bees and Hill, 1998). Here, ν , ρ , V_n and τ are cell volume, density, mean swimming speed and direction correlation time, respectively, $\Delta \rho$ is the difference between cell and fluid density, g is the gravitational acceleration and N is the scaled mean cell concentration (Williams and Bees, 2011). The case $\chi = 0$ is for zero or red light; a gyrotaxis-only model (Bees and Hill, 1998). Increasing χ is equivalent to increasing light intensity; however, I_c is not known, so quantitative conversion between the two is not possible. The linear stability analysis provides an estimate for the critical Rayleigh number Ra_c and corresponding critical wavenumber k_c ; for $Ra < Ra_c$ small perturbations decay; for Ra just greater than Ra_c , instabilities develop with a wavenumber of k_c . (Note: the critical dimensional wavelength λ_c is given by $2\pi H/k_c$.) Experiments provide an estimate of the dominant initial wavelength, λ_0 , which has a non-zero growth rate and occurs for some $Ra > Ra_c$. We may compare the predicted critical wavelength λ_c at $Ra = Ra_c$ with the fastest growing wavenumber, λ_0 , as experimental I or theoretical χ are varied, as long as Ra is not too much greater than Ra_c .

For the comparison, we fix $H = 0.306 \text{ cm}$ and the direction correlation time $\tau = 5 \text{ s}$ (Bees and Hill, 1997), the gyrotactic reorientation time scale $B = 6.3 \text{ s}$ (Jones et al., 1994) and the dimensional measure of absorbance $\alpha = 3.67 \times 10^7 \text{ cm}^2$ (*C. augustae*;

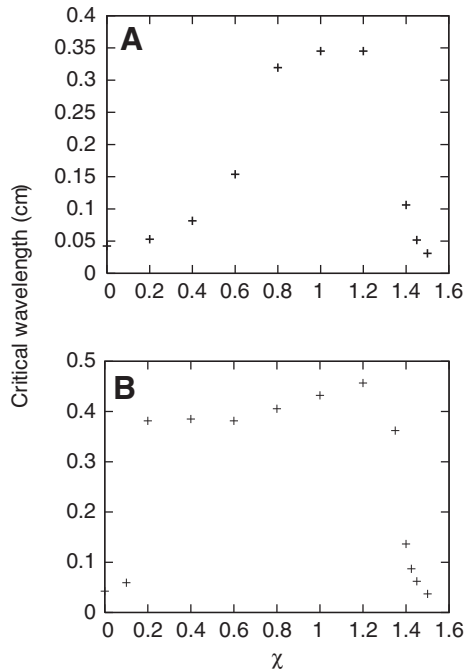


Fig. 10. Critical wavelength, λ_c , plotted against χ for (A) model A and (B) model B. $H=0.306$ cm; $\alpha=3.67 \times 10^7$ cm².

colorimeter measurement). Using these parameters, the theoretical predictions provide λ_c and Ra_c , which are shown along with the experimental data in Table 5.

We find promising consistency between theoretically predicted critical wavelengths and experimentally observed dominant initial wavelengths. The critical wavelength in the dark is $\lambda_c=0.042$ ($Ra_c=2.77 \times 10^6$), which is approximately a factor of four lower than the measured wavelength $\lambda_0=0.190$ for red light data (at a fixed $Ra=2.18 \times 10^6$). Models A and B predict an increase in λ_c initially with increasing χ followed by a decrease for some value of $\chi > 1$, a trend also seen in the experimental data for λ_0 as I increases (compare

Figs 8 and 10). The critical wavelength does not vary much once the maximum value of λ_c is reached, until $\chi > 1.25$. The maximum critical wavelength and critical Rayleigh number are $\lambda_c=0.345$ cm and $Ra_c=1.49 \times 10^5$ in Model A, and $\lambda_c=0.457$ cm and $Ra_c=2.20 \times 10^5$ in Model B, respectively. In the experimental data, the maximum λ_0 ranged from 0.244 to 0.262 cm for $I=1330$ lx over the three experiments. In Models A and B, the critical wavelength decreases rapidly and nonlinearly as $\chi > 1.25$ increases. The analogous decrease in λ_0 is linear in the experiments. This may be due to the models having the same critical light intensity, I_c , for all cells, whereas a natural distribution of I_c in experiments would act to smooth the transition. We see a larger range for λ_c than was found experimentally for λ_0 , which may in part be due to the fact that the critical wavelength is not necessarily representative of the fastest growing mode; this is especially true for large critical wavelengths (small wavenumbers).

To conclude, comparisons between theoretical and experiment results are difficult and there are many limitations. Experimentally identifying the very first dominant wavelength can be difficult, and there will always be remnants of the mixing. Theoretically, the prediction of λ_c comes from finding a steady distribution and perturbing, but there may not be sufficient time for the formation of this state. The aim of the work was to explore mechanisms rather than using parameter-fitting methods. We have observed qualitative agreement between experiments and theory, and anticipate quantitative alignment once better parameter measurements are obtained and the theoretical analyses refined.

Conclusions

In this paper, we have developed and employed techniques to quantify the initial pattern wavelength of bioconvection as a function of concentration and light intensity in a repeatable fashion. A novel mixing methodology was developed to create a consistently uniform distribution before the onset of pattern formation. In practice, this is a difficult task and the distribution is never uniform; the mixing can never be perfect and the swimming behaviour of the cells relative to the fluid flow induces memory. However, the employed on-off series of rotations were vigorous, inducing large amplitude flows that decayed rapidly and mixing the cells thoroughly and quickly. In all but a few cases where pattern formation was rapid (very high

Table 5. Summary of experimental results and theoretical predictions, with illumination from above

	I (lx)	λ_0 (cm)	Ra ($\times 10^6$)
Experiment			
RA	Any/0	0.190	2.18
LA1	645	0.235	2.18
LA1	1330	0.256	2.18
LA1	2020	0.228	2.18
LA1	2710	0.201	2.18
LA1	3390	0.188	2.18
LA1	4080	0.170	2.18
LA1	4780	0.159	2.18
Theory			
No light	χ	λ_c (cm)	Ra_c ($\times 10^6$)
Model A/B	0	0.042	2.77
Model A/B	0.6	0.154/0.381	1.32/0.717
Model A/B	1.0	0.345/0.432	0.402/0.317
Model A/B	1.2	0.345/0.457	0.271/0.236
Model A/B	1.4	0.106/0.136	10.9/11.6
Model A/B	1.45	0.051/0.062	36.3/39.5
Model A/B	1.5	0.031/0.037	91.6/101.0

The layer depth (H) was 0.306 cm for all experiments and results from theories.

I , light intensity; λ_0 , initial wavelength; λ_c , critical wavelength; Ra , Rayleigh number; Ra_c , critical Rayleigh number; χ , ratio of light intensity at the source to critical light intensity.

concentrations), the patterns did not display any structure associated with remnants of the mixing protocol, and developed from a steady and uniform suspension. Furthermore, the mixing regime ensures that the initial conditions are at least consistent between runs, allowing changes in the wavelength to be attributed to culture parameters. Future work could attempt to quantify the mixing (but note that it does not follow that the mixing of tracer particles is equivalent to the mixing of gyrotactic swimming cells).

Images were captured and the dominant initial pattern wavelength was extracted using Fourier analysis. The trend in initial wavelength as a function of concentration was similar to that found previously (Bees and Hill, 1997). Red light illumination at 660 nm was found to have no effect on initial pattern wavelength. However, significant trends for initial wavelength as a function of white light illumination from either above or below were discovered, analysed and interpreted. In particular, the competition between gravitaxis, gyrotaxis and phototaxis proved to be fundamental to the pattern-forming process. Comparisons between a new photo-gyrotactic theory (Williams and Bees, 2011) (incorporating the Lambert–Beer law for light absorption) and these experimental results were made, indicating some good agreement. To extend the comparison to long-term pattern wavelengths for the photo-gyrotactic system, it will be necessary to take into account the likely nonlinear scattering that will occur locally within downwelling plumes with significantly higher cell concentrations than the mean. Refinement of the trends around what appear to be the critical values of I should also be explored to try and provide an accurate estimate of I_c . Techniques should be developed to analyse geometrical aspects of the patterns under different illumination conditions, and so elucidate the mechanisms at play during photo-gyrotactic bioconvection.

LIST OF SYMBOLS AND ABBREVIATIONS

BBM	Bold's basal medium
C	concentration
d	scaled layer depth
E	Ekman number
FFT	fast Fourier transform
H	layer depth
I	light intensity
I_c	critical light intensity
k_0	initial wavenumber
k_c	critical wavenumber
k_d	dominant wavenumber
Ra	Rayleigh number
Ra_c	critical Rayleigh number
t_0	time from mixing to pattern formation
v	volume
W_1	image width
α, β, c	fitting parameters in the double logarithmic function

χ	dimensionless ratio of critical to source intensity
λ_0	initial wavelength
ν	viscosity
$ \Omega $	vortex mixer speed
τ	direction correlation time

ACKNOWLEDGEMENTS

The authors gratefully acknowledge support from the EPSRC (EP/D073398/1).

REFERENCES

- Acheson, D. J. (1990). *Elementary Fluid Dynamics*. Oxford: Oxford University Press.
- Bees, M. A. and Hill, N. A. (1997). Wavelengths of bioconvection patterns. *J. Exp. Biol.* **200**, 1515–1526.
- Bees, M. A. and Hill, N. A. (1998). Linear bioconvection in a suspension of randomly swimming, gyrotactic micro-organisms. *Phys. Fluids* **10**, 1864–1881.
- Bees, M. A., Hill, N. A. and Pedley, T. J. (1998). Analytical approximations for the orientation distribution of small dipolar particles in steady shear flows. *J. Math. Biol.* **36**, 269–298.
- Childress, S., Levandowsky, M. and Spiegel, E. A. (1975). Pattern formation in a suspension of swimming microorganisms: equations and stability theory. *J. Fluid Mech.* **69**, 591–613.
- Cziroák, A., Janosi, I. M. and Kessler, J. O. (2000). Bioconvective dynamics: dependence on organism behaviour. *J. Exp. Biol.* **203**, 3345–3354.
- Foster, K. W. and Smyth, R. D. (1980). Light antennas in phototactic algae. *Microbiol. Rev.* **44**, 572–630.
- Ghorai, S. and Hill, N. A. (2005). Penetrative phototactic bioconvection. *Phys. Fluids* **19**, 74–101.
- Häder, D. P. (1987). Polarotaxis, gravitaxis and vertical phototaxis in the green flagellate, *Euglena gracilis*. *Arch. Microbiol.* **147**, 179–183.
- Hill, N. A. and Häder, D. P. (1997). A biased random walk model for the trajectories of swimming micro-organisms. *J. Theor. Biol.* **186**, 503–526.
- Hill, N. A., Pedley, T. J. and Kessler, J. O. (1989). Growth of bioconvection patterns in a suspension of gyrotactic micro-organisms in a layer of finite depth. *J. Fluid Mech.* **208**, 509–543.
- Jones, M. S., le Baron, L. and Pedley, T. J. (1994). Biflagellate gyrotaxis in a shear flow. *J. Fluid Mech.* **281**, 137–158.
- Kessler, J. O. (1984). Gyrotactic buoyant convection and spontaneous pattern formation in algal culture. In *Non-equilibrium Cooperative Phenomena in Physics and Related Fields* (ed. M. G. Verlarde), pp. 241–248. New York: Plenum.
- Kessler, J. O. (1985a). Co-operative and concentrative phenomena of swimming micro-organisms. *Contemp. Phys.* **26**, 147–166.
- Kessler, J. O. (1985b). Hydrodynamic focusing of motile algal cells. *Nature* **313**, 218–220.
- Kessler, J. O. (1986). The external dynamics of swimming micro-organisms. *Prog. Phycol. Res.* **4**, 258–305.
- Kessler, J. O., Hill, N. A. and Häder, D. P. (1992). Orientation of swimming flagellates by simultaneously acting external factors. *J. Phycol.* **28**, 816–822.
- Nultsch, W., Throm, G. and von Rimscha, I. (1971). Phototaktische untersuchungen an *Chlamydomonas reinhardtii* dangeard in homokontinuierlicher kultur. *Arch. Mikrobiol.* **80**, 351–369.
- Pedley, T. J. and Kessler, J. O. (1990). A new continuum model for suspensions of gyrotactic micro-organisms. *J. Fluid Mech.* **212**, 155–182.
- Platt, J. R. (1961). "Bioconvection Patterns" in cultures of free-swimming organisms. *Science* **133**, 1766–1767.
- Veronis, G. (1963). Penetrative convection. *J. Astrophys.* **137**, 641–663.
- Vincent, R. V. and Hill, N. A. (1996). Bioconvection in a suspension of phototactic algae. *J. Fluid Mech.* **327**, 343–371.
- Wager, H. (1911). On the effect of gravity upon the movements and aggregation of *Euglena viridis*, Ehrb. and other micro-organisms. *Philos. Trans. R. Soc. Lond. B* **203**, 333–390.
- Williams, C. R. (2009). Pattern formation and hydrogen production in suspensions of swimming green algae. PhD thesis, University of Glasgow, Glasgow, UK.
- Williams, C. R. and Bees, M. A. (2011). Photo-gyrotactic bioconvection. *J. Fluid Mech.* doi:10.1017/jfm.2011.100, 1–46.